Theor Chem Acc (2006) 115: 196–203
DOI 10.1007/s00214-005-0059-z

REGULAR ARTICLE

Francisco Torrico · Rafael R. Pappalardo
Enrique Sánchez Marcos · José M. Martínez

Hydration structure and dynamic properties of the square planar Pt(II) aquaion compared to the Pd(II) case

Received: 15 July 2005 / Accepted: 3 September 2005 / Published online: 17 December 2005

Abstract This work examines, by means of classical Molecular Dynamics simulations, the hydration of a square planar hydrate, $[Pt(H_2O)_4]^{2+}$, focussing the attention on the structure and dynamics adopted by water molecules in the regions above and underneath the molecular plane. Results obtained are compared with those previously derived for the case of the $[Pd(H_2O)_4]^{2+}$ where the concept of *meso-shell* was introduced to define this axial region [Martínez et al. (J Phys Chem B 108:15851, 2004)]. Specific ab initio intermolecular potentials describing the interaction between the ion and the solvent have been developed following the statistical implementation of the hydrated ion concept for the case of a planar aquaion. A meso-shell is characterized by a peak in the Pt–O RDF centered at 2.95 Å which integrates to two water molecules; the mean residence time for these molecules is in the range 1–7 ps. The vibrational frequency associated to the dynamic variable defined from the distance meso-shell water molecule-cation is used to quantify the linkage degree of the water molecule in this shell. The meso-shell in Pt(II) is more labile than in the Pd(II) case, whereas the first and second hydration shells of both cations are highly similar. The observed differences in meso-shell are discussed in relation with the mechanistic interpretation of the solvent exchange at the first hydration shell.

Keywords Pd(II) · Pt(II) · hydrated ion · meso-shell · molecular dynamics

1 Introduction

The importance of the hydration phenomenon in the understanding of the aqueous solution chemistry of metal ions is well established [1–4]. The distribution that the nearest solvent molecules adopt around the ions largely depends on the nature of the ion and in most of the cases well-defined structures for the water molecules surrounding the cation are observed defining what is known as hydrated ion (HI) or aquaion, i.e. the $[M(H_2O)_m]^{n+}$ species [5]. In spite of its apparent simplicity, much of the coordination chemistry and reactivity of the ions in more complex structures, like those present in biochemical systems [6], where total or partial dehydration is usually observed, can be correlated [7,8] with the structural and energetic features of the aquaion and the solvent molecules *hydrating* the aquaion, i.e. the second hydration shell [9,10].

Theoretical (quantum chemistry and statistical simulations) and experimental (neutron diffraction, X-ray diffraction and X-ray absorption) techniques have provided in the last three decades a large body of knowledge concerning structural arrangements adopted by the solvent for most of the metal ions in aqueous solutions [1,2,11]. However, the available information for Pd^{2+} and Pt^{2+} ions is still scarce. The d^8 electronic configuration of these two ions favors a square planar arrangement for the aquaion $[M(H_2O)_4]^{2+}$ ($M = Pd^{2+}, Pt^{2+}$) with virtually the same metal–oxygen distance, ∼2.00–2.02 Å range, for both ions [2,12–16]. For the Pd(II) case, two recent works [14,15] have been published providing a new picture for the hydration pattern of this ion. One of the more striking results concluded in our theoretical work [14], based on molecular dynamics simulations, is the presence of two axial water molecules loosely coordinated to the ion not previously reported by Hellquist applying extended X-ray absorption fine structure spectroscopy EXAFS [16]. These two solvent molecules, occupying the axial regions above and below the molecular plane, bear structural and dynamic properties in between those typically observed for *classical* first and second hydration shells. They also do not follow the Frank and Evans [9] picture where the solvent adopts a structure around the ion in concentric shells. This new hydration pattern compelled us to propose the new term meso-shell to identify these solvent molecules. The EXAFS work published later by Purans et al. [15] also reports the presence of two weakly bound water molecules. For the Pt(II) case, in spite of the mentioned close similarity of the HI structures, the two published EXAFS works [13,

F. Torrico · R.R. Pappalardo · E.S. Marcos · J.M. Martínez (✉)
Departamento de Química Física, Facultad de Química,
Universidad de Sevilla, 41012 Sevilla, Spain
E-mail: josema@us.es

16] on aqueous solutions coincide in the absence of water molecules occupying the axial regions. It is worth mentioning that in this case the experimental work is more involved due to the low yield produced in the synthesis process [2] of the Pt(II) aquaion (solutions of mM concentration).

The elucidation of the axial coordination for these two aquaions is an important issue, particularly for the interpretation of the ligand exchange mechanisms [17–19]. In this sense, ligand substitution rates differ between Pd(II) and Pt(II) by six orders of magnitude in the case of the water exchange ($k_{ex}^{Pd^{2+}}/k_{ex}^{Pt^{2+}} \approx 10^6$, k_{ex} being the water exchange rate at 298 K). This differential behavior, attributed to an activation enthalpy ($\Delta H^{\neq}$) for platinum larger than for palladium [18], is also observed in other species of high medical interest due to their use as anticancer drugs. Reactive forms of Pt-based drugs are recognized [20,21] to be produced by means of a hydrolysis process where the original ligands coordinating the ion are substituted by water inside the cell medium producing aquated Pt(II) species. The anticancer activity difference observed for palladium and platinum homologues has been attributed to the difference in the hydrolysis of the leaving groups, that takes place too fast for Pd(II) to reach the pharmacological targets [22]. Therefore, the knowledge of the most simple aquated species in solution of these two ions, namely the aquaions, seems to be a necessary basic step in order to understand their differences.

The present work aims to provide new insights from a theoretical approach about structural, energetic and dynamic features of the Pt(II) hydration phenomenon. That could also be of help for understanding the experimental differences observed, compared to Pd(II), in the *detection* of axial solvent molecules coordinating the ion.

2 Methods

Molecular dynamics simulations presented in this work are based on the use of the HI concept to model the cation–water interactions [23,24]. The high perturbation (electronic and nuclear polarizations and charge transfer effects) exerted by the metal ion on the water molecules directly interacting with it, allows to distinguish them from the rest of the solvent. In the case studied, the aquaion $[Pt(H_2O)_4]^{2+}$ is adopted as the representative entity in solution and the description of the interactions involving the cation is performed through the definition of two interaction potentials [25]: one for the hydrated ion–water (HIW) forces and one for the internal dynamics of the aquaion [ion water first shell (IW1)]. We have established a first principles strategy where the needed potentials have been successfully developed and applied for several multiple charged metal ions with tetrahedral and octahedral environments [25–27]. Two relevant advantages are derived from this strategy. On one hand, the HI approach to implement the intermolecular potentials implies that the ion–solvent interactions accounting for the important many-body effects [28] present in the ion neighborhood are taken into account in an effective way, allowing the low cost pairwise additive scheme for the force evaluation to be still suitable. On the other hand, molecular dynamics simulations provide the intrinsic statistical nature of the aqueous solutions. The model was recently extended [14] to the more involved case of the Pd^{2+} square planar geometry and the same methodology is applied here for Pt^{2+}. A premise to be fulfilled by the cation is that the water release process for the first hydration shell must be slow enough, compared to the simulation time (ns range). The current implementation of the HI model does not allow the description of the water exchange that implies an on-the-fly change in the interaction potentials of the leaving and entering solvent molecules. Pt(II) ion is suitable for the HI methodology because mean lifetime for first shell water molecules is above 1 h, that is, several orders of magnitude above the simulation times.

2.1 Interaction potentials

Two different interaction potentials, working on different space regions, have been developed in order to perform the aqueous MD simulations containing the aquaion $[Pt(H_2O)_4]^{2+}$. The $IW1_{SP}$ potential defines the interaction between the cation and the first shell water molecules, and together with the appropriate water–water interactions [25, 26], governs the internal dynamics of the HI. The interaction between the HI and the rest of the solvent molecules, i.e. bulk solvent, is described by means of the HIW_{SP} potential. The subscript SP indicates that the model is applied to a square planar geometry.

These two interaction potentials are obtained by fitting interaction energies computed at MP2 level. Platinum atom has been described by means of the SDD pseudopotential of the Stuttgart group [29] and for the oxygen and hydrogen atoms, the aug-cc-pvdz basis sets [30] were employed. In order to obtain the IW1 potential, ca. 70 deformations of the reference structure, D_4 symmetry, following stretching and bending normal mode patterns were performed. It is worth mentioning that two additional sites (X) were defined above and below the molecular plane defining, together with the metal ion, a rigid unit. These two new sites help in maintaining an average planar structure along the simulation due to the interactions with the water molecules belonging to the aquaion. In addition, its use allows a better description of the interaction of the HI with bulk solvent molecules when they are positioned in the axial regions. The functional form used for the IW1 potential is the following:

$$E_{IW1_{SP}} = \sum_{i}^{PtX_2\ sites} \frac{C_4^{iO}}{r_{iO}^4} + \frac{C_6^{iO}}{r_{iO}^6} + \frac{C_8^{iO}}{r_{iO}^8} + \frac{C_{12}^{iO}}{r_{iO}^{12}} + \sum_{j}^{water\ sites} \frac{q_{Pt} q_j}{r_{Pt-j}}. \quad (1)$$

Water–water interactions inside the HI are defined according to the TIP4P [31] potential for the Lennard–Jones part. The electrostatic part of the interaction is defined according to the CHELP [32] charges obtained for the D_4 ref-

erence structure including the solvent polarization on the wavefunction by means of the dielectric continuum PCM methodology [33,34]: $q_{Pt} = 1.03$ ue, $q_O = -0.88$ ue, $q_H = 0.56$ ue.

The HIW potential is obtained by fitting the form

$$E_{HIW_{SP}} = \sum_{i}^{\text{HI sites}} \sum_{j}^{\text{water sites}} \frac{D_4^{ij}}{r_{ij}^4} + \frac{D_6^{ij}}{r_{ij}^6} + \frac{D_{12}^{ij}}{r_{ij}^{12}} + \frac{q_i q_j}{r_{ij}} + A_{ij} \cdot e^{-B_{ij} r_{ij}} \quad (2)$$

to ca. 600 $[Pt(H_2O)_4]^{2+}$–H_2O interaction energies in which the probe water molecule samples different positions and orientations around the reference tetrahydrate structure. Table 1 collects the fitted coefficients for the $IW1_{SP}$ and HIW_{SP} interaction potentials. Further details about the interaction potential built for aquaions exhibiting a square planar geometry can be found in Ref. [14].

Finally, it is worth mentioning that a quantum mechanics geometry optimization of the tetrahydrate and a water molecule initially sitting along the axial direction produces a final arrangement in which the water molecule migrates to the equatorial region in which first–second shell hydrogen bond interactions can be recognized. This result, previously reported [13], reflects the absence of minima along the axial direction for the $[Pt(H_2O)_4H_2O]^{2+}$ aggregate. If the minimization is performed using the HIW_{SP} and $IW1_{SP}$ interaction potentials, the same result is obtained. This agreement is important because it reflects that no bias has been introduced in the description of the ion–solvent interactions in the axial region by using the new potentials.

Table 1 Fitted coefficients for the $IW1_{SP}$ and HIW_{SP} interaction potentials (energies in kcal/mol and distances in Å)

Coefficient	Value
$IW1_{SP}$ potential	
C_4^{Pt-O}	−36, 462.69
C_6^{Pt-O}	−192, 090.03
C_8^{Pt-O}	359,592.07
C_{12}^{Pt-O}	24,034.97
C_4^{Pt-H}	0.00
C_6^{Pt-H}	0.00
C_8^{Pt-H}	0.00
C_{12}^{Pt-H}	0.00
C_4^{X-O}	15,735.25
C_6^{X-O}	106,980.62
C_8^{X-O}	−190, 444.06
C_{12}^{X-O}	683.85
HIW_{SP} potential	
D_4^{Pt-O}	3,776.71
D_6^{Pt-O}	−15, 669.21
D_{12}^{Pt-O}	−13, 624, 849.98
D_4^{Pt-H}	54.93
D_6^{Pt-H}	−1, 222.29
D_{12}^{Pt-H}	7,367.44
D_4^{X-O}	0.00
D_6^{X-O}	22,097.36
D_{12}^{X-O}	5,234,494.01
D_4^{X-H}	0.00
D_6^{X-H}	692.13
D_{12}^{X-H}	−2, 581.34
A_{X-O}	−8, 016.72
B_{X-O}	1.88
A_{X-H}	−84.03
B_{X-H}	0.92
$r(Pt - X)$	0.10

2.2 Molecular dynamics simulation details

Molecular dynamics simulations at 300 K were performed with the MOLDY code [35,36] in the canonical ensemble (NVT) using periodic boundary conditions. The simulation cell, containing 1 $[Pt(H_2O)_4H_2O]^{2+}$ plus 496 TIP4P [31] water molecules, reproduces a density of 1 g/cm^3. An equilibrated structure of the previous Pd(II) simulation [14] was used as starting configuration and after a short equilibration period, a timestep of 2 fs was applied and atomic positions and velocities saved every two steps during 500 ps for further analysis. Ewald sum methodology [37] was applied to account for the electrostatic interactions, including the charged system term [38,39]. Simulations with net charged cells can be performed using an energy correction term that is physically equivalent to adding a uniform jelly of charge that exactly neutralizes the total cell charge [40]. Although more sophisticated corrections have been proposed [41], these concern simulations in which the volume, the system shape, or the net charge is altered during the simulation process. None of those cases apply to the simulations presented here.

3 Results and discussion

3.1 Structure

Metal–oxygen and metal–hydrogen radial distribution functions are shown in Fig. 1. For comparative reasons the same distributions obtained for Pd(II) [14] are also included. Pt–O RDF shows three well-defined maxima located at 2.02, 2.95 and 4.08 Å, respectively. The first sharp peak reflects the well-defined distribution of the four water molecules defining the tetrahydrate while mainly second hydration shell water molecules contribute to the third one. The second peak integrates to two solvent molecules. The Pd–O distribution is extremely similar to that of the platinum except for the middle peak, that is sharper and appears at a shorter distance, 2.67 Å. This particular maximum corresponds to the two axial water molecules that, although present in both distributions, are clearly

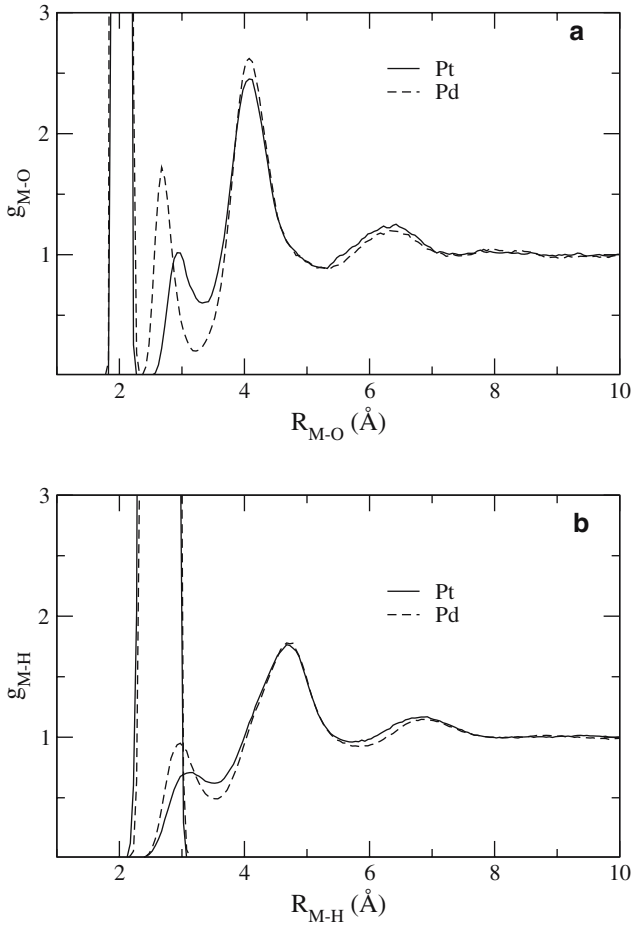

Fig. 1 M–O (**a**) and M-H (**b**) radial distribution functions

less well defined in the case of platinum. The M–H distributions also evidence the presence of the three mentioned water shells. An analysis of the orientational parameter (not shown) provides an average value of 100° for the angle defined by M–O and water dipole vectors for the water molecules occupying the axial region. In the case of the molecules defining the third peak of the Pt–O RDF, that value is 123°. These values show how water molecules coordinating the ion through the axial region, in spite of being closer to the metal cation compared to the equatorial second hydration shell, are not more structurally conditioned by the electric field created by the metal ion than the water molecules at the second shell. For the Pd^{2+} ion, the value reported for the axial solvent molecules was 110°, so the new pattern where distance and orientation do not follow a monotonic function is now even more evident. The orientational tendency of the water molecules occupying the meso-shell must be understood on the basis of a hydrogen-bonded network, in which the solvent molecule occupying the axial position defines its relative orientation according to the hydrogen bond interactions with the surrounding water molecules. Fig. 2 shows a randomly chosen snapshot where the hydrogen-bonded network involving the axial water molecules is visualized.

3.2 Dynamics

Mobility of the Pt^{2+} ion and second shell water molecules in terms of the self-diffusion coefficient (D) have been estimated from the slope of the corresponding mean square displacements and from the integration of the velocity autocorrelation functions [37]. Both approaches provide estimates whose differences are below the statistical uncertainties. Table 2 also collects the results obtained for Pd^{2+}. Unfortunately, no experimental determination of $D_{Pt^{2+}}$ has been found in the literature, so we limit here to the comparison between both ions. The diffusion dynamics for Pd(II) and Pt(II) ions and their corresponding second hydration shells is the same. If the second hydration shell mobility is compared with that reported for a more tightly joined shell, like the Cr^{3+} one [25], the mobility is now increased by ca. 50%. In the case of palladium, it has been possible to estimate the self-diffusion coefficient of the meso-shell, while for platinum, the higher lability of the water molecules defining that shell (see next section) does not allow a reliable estimation of the property. Interestingly, the meso-shell diffuses slower than the second hydration shell, showing a behavior that is closer to that of the ion. In this sense, and in contrast to other structural properties, such as the orientational parameter, or dynamical properties, such as mean residence times (Table 3), a well-defined pattern is found for the solvent mobility and the distance to the ion:

$$D_{\text{cation}} < D_{\text{meso-shell}} < D_{\text{second shell}}$$

A magnitude providing information about the lability of the solvation shells is the mean residence time (τ) of the solvent molecules. Calculations for the meso-shell and the second hydration shell have been performed according to the method of Impey et al. [42] and results are shown in Table 3. Again, hardly observable differences are found for the second hydration shells of palladium and platinum, in agreement with the discussed radial distribution functions and the mobilities. However lower persistence of the solvent molecules in the axial region is evidenced for Pt(II), telling us that, although on average two axially located water molecules coordinate Pt^{2+}, the lability is higher compared to the case of Pd^{2+}. Therefore water exchanges in that region happen more frequently for Pt(II) and this can be observed by the axial coordination number distributions of Fig. 3. The broader distribution obtained for this ion involves more transient situations with higher or smaller (than two) number of solvent molecules simultaneously occupying the axial sites. Anyhow, the difference in size for both meso-shell and second hydration shell regions is a factor to take into account: while a diffusive motion within the second hydration shell is possible, that is not the case for the meso-shell.

The low definition of the meso-shell according to the Pt–O RDF and the high lability shown by the mean residence times can lead us to question whether the well-defined meso-shell observed in the neighborhood of the Pd^{2+} ion is still present in the case of platinum. In other words, when a solvent molecule occupies an axial coordination site, is it really interacting with the cation? or simply, it is sitting

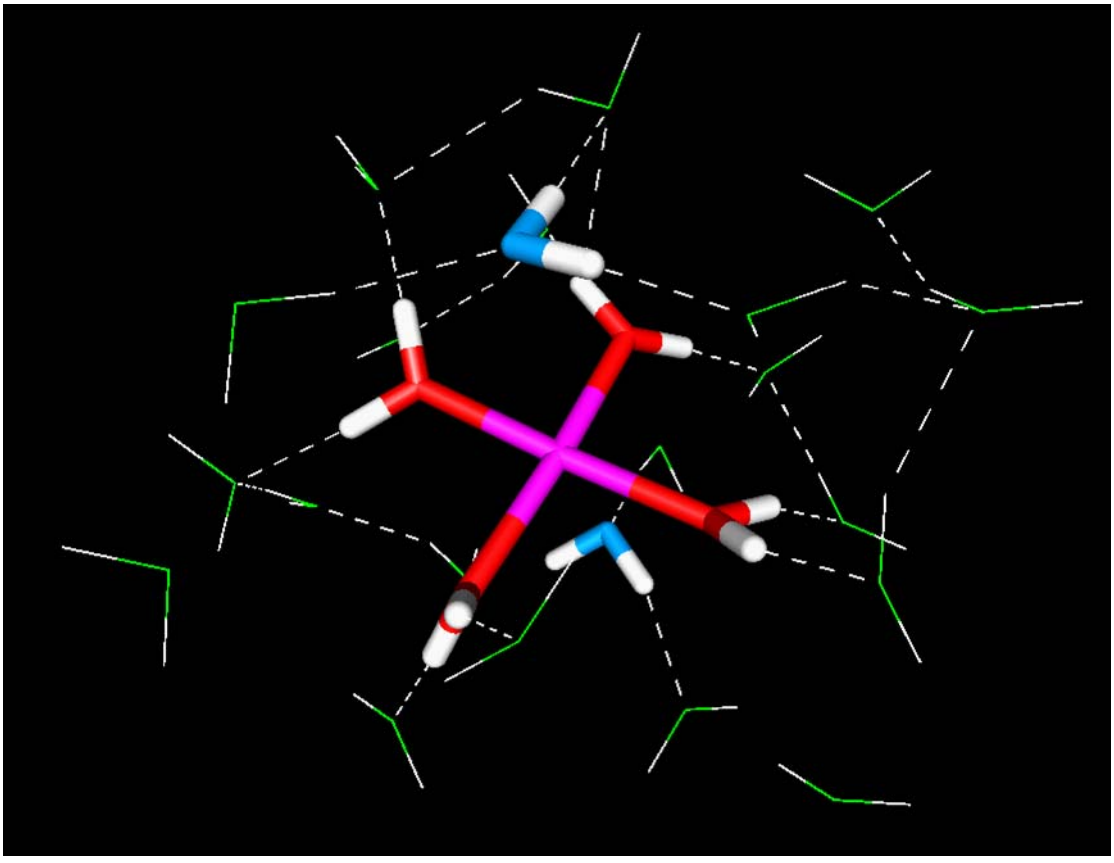

Fig. 2 Snapshot taken from the Pt(II) simulation where the hydrogen bond network involving the axially located water molecules (*blue colored*) can be observed. First shell water molecules are *red colored* and the rest of water molecules are *displayed as wires*

Table 2 Diffusion coefficients (10^{-5} cm^2/s)

	Pd^{2+} simul.	Pt^{2+} simul.
Ion	0.67 ± 0.05	0.68 ± 0.1
Meso-shell	0.83 ± 0.05	–
Second shell	1.5 ± 0.1	1.6 ± 0.1

Table 3 Mean residence times (ps)

	Meso-shell		Second shell	
	Pd(II)	Pt(II)	Pd(II)	Pt(II)
$t^* = 0$ ps	4	1	12	9
$t^* = 2$ ps	10	7	19	18

t^* defines the maximum transient period a solvent molecule can temporarily leave a specific region without loosing its ascription [42]

there because that region is energetically favorable but the molecule mainly responds to the solvent hydrogen bond network dynamics. If the solvent–HI *complex* is certainly defined, that entity should survive to several vibrations, and more, these should be observed during the life time of the complex. Such a kind of detailed information is accessible from the molecular dynamics simulations where time evolution of all the particles is available. Figure 4 shows, for palladium and platinum, the distance between the cation and the center of mass of one of the found solvent molecules that occupies one of the two axial coordination sites for a period of at least 3 ps. This time period has been chosen on the basis of a compromise between the computed mean residence times for both ions (see Table 3) and a statistically significant interval for the range of observed frequencies. As a consequence several vibrations can be observed and no different behavior between palladium and platinum is observed in this concern. If the Fourier transform of the autocorrelation function associated to the dynamic variable $r_{M-O}(t)$ is computed, the characteristic frequency of the corresponding vibration is obtained [26]. The frequencies obtained for the meso-shell water molecules are 175 and 130 cm^{-1} for palladium and platinum, respectively. These values are considerably lower than the ones obtained for the ion-water first shell vibration if the same kind of analysis is performed: 528 cm^{-1} for Pd(II) and 575 cm^{-1} for Pt(II). Unfortunately, no IR/Raman experimental studies of the aquaions are reported in the literature. These results clearly indicate the lower force constants associated to the M–O vibrations involving the water molecules occupying the meso-shell region. Anyhow, it can be stated, according to these evidences, that the meso-shell is also present in the hydration structure around the Pt(II) ion, although not as well structurally defined as in the case of Pd(II).

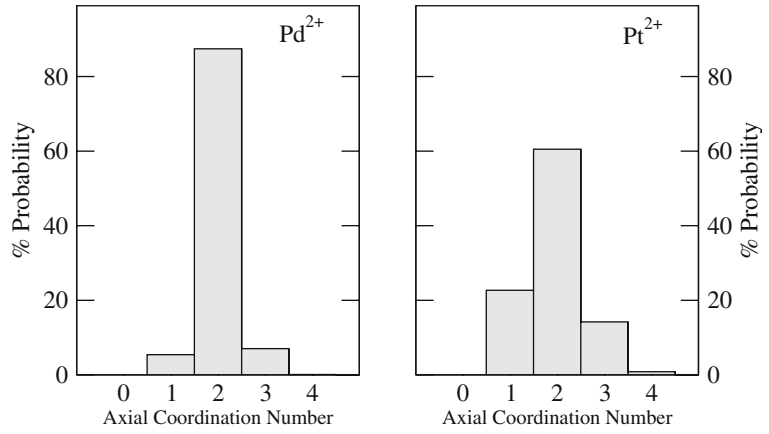

Fig. 3 Axial coordination number distributions obtained from Pd^{2+} and Pt^{2+} aqueous simulations

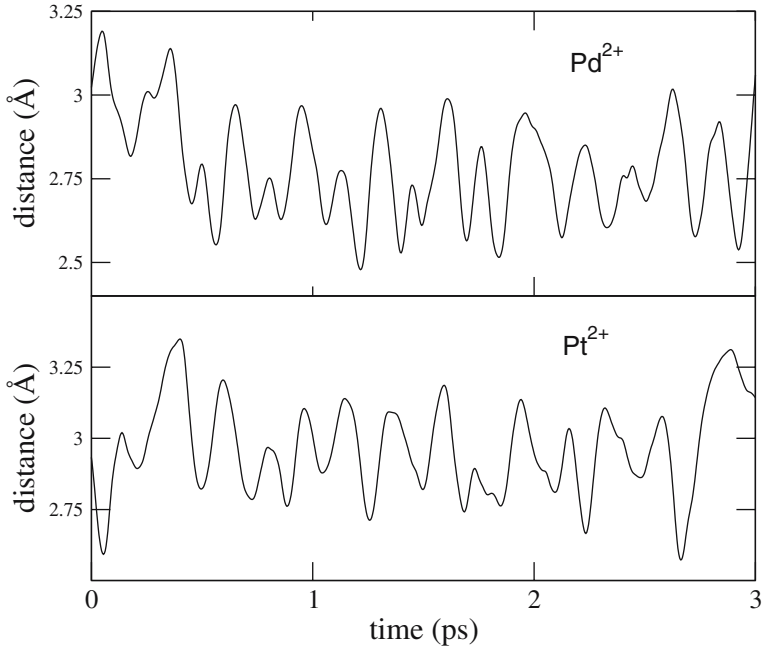

Fig. 4 Time evolution of the ion–water distance for one of the water molecules axially coordinating the ion for a period of 3 ps

3.3 Energetics

In order to quantify from an energetic point of view the observed similarities and differences between the hydration structures of Pd^{2+} and Pt^{2+} ions, an analysis of the interaction energies between the HI and the meso- and second hydration shells have been performed. One thousand two hundred and fifty clusters equally spaced in time were selected from each of the Pd(II) and Pt(II) aqueous simulations. Water molecules up to the second hydration shell, according to the M–O RDF, were included in the sets. For each cluster the interaction energy of the HI with the meso-shell and with the second hydration shell water molecules were computed. The average interaction energy, computed using the developed potentials, per water molecule is reported in Table 4; it is observed that palladium aquaion interacts more strongly with the axial shell than platinum aquaion does, while the same average interaction energy is found for both ions concerning the second hydration shell. This unlike energetics may be the origin of the observed differences between both ions. Although a polarizable water model could certainly improve the quality of the simulations, the HI strategy highly

Table 4 Interaction energies (kcal/mol) per water molecule between the hydrated ions and the solvent molecules occupying the axial and second hydration shell regions

	Pd^{2+}	Pt^{2+}	ΔE^a
Meso-shell	-11.5 ± 3	-8.3 ± 4	-3.2
Second shell	-13.2 ± 1	-13.2 ± 1	0.0

[a] $\Delta E = E_{int}(Pd^{2+}) - E_{int}(Pt^{2+})$

reduces the many-body effects present in the neighborhood of the ion. Therefore, compared to the present results, only qualitative differences could be expected from a more involved water model.

3.4 The meso-shell and its experimental detection

A proper technique for describing the ion environment in dilute aqueous solutions is EXAFS [43]. Contributions from the atoms surrounding the absorber (metal ion in our case) to the EXAFS signal are summed up by shells (j) of equivalent back-scatterer atoms according to the expression [43]:

$$\chi(k) = \sum_j \frac{N_j S_o^2}{k\bar{R}_j^2} |f_j^{\text{eff}}(k)| \sin(2k\bar{R}_j + \varphi(k)) \; e^{-2\bar{R}_j/\lambda(k)} e^{-2\sigma_j^2 k^2}, \quad (3)$$

k being the photoelectron wave vector, that is, the energy of the ejected photoelectron. Each contribution can be understood as an oscillatory signal multiplied by an amplitude factor. For each shell, the simulation analysis yields straightforward estimations for all the following parameters: N: number of equivalent atoms in a given shell; $\bar{R}$: average distance for the atoms defining a shell; σ: Debye–Waller factor that measures the thermal and structural disorder in a shell.

With all this information the envelope

$$\frac{N}{k\bar{R}^2} e^{-2\sigma^2 k^2} \quad (4)$$

of the oscillatory shell signal contribution can be computed directly from the simulation. Although some factors present in Eq. (3) are not taken into account, the main differences between the different shells come from the above envelope, specially if the type of back-scatterer is the same (oxygen in our case). The parameters obtained in this work are collected in Table 5 and for comparative purposes those of the well-defined second hydration shell of Cr^{3+} [44], and the ones obtained from Purans et al. [15] for the palladium axially coordinating water molecules are also included. In Fig. 5 the different envelopes are plotted. The amplitude resulting from the use of the palladium simulation parameters is very similar to that experimentally determined by Purans work, and larger than that corresponding to platinum. The marginal contribution the meso-shell makes to the total EXAFS signal is also evident, if the first hydration shell contribution (the largest one in the analysis process) is taken as reference. The amplitude of the second shell contribution in the case of Cr(III) [44] is in between the first- and meso-shell ones, and, before the Purans results, was accepted as the limiting contribution accessible through EXAFS for aqueous environments in ionic solutions [44–46]. Taking into account that not all the parameters of Eq. (3) have been considered in this analysis and the fact that in Eq. (3) only single scattering contributions are taken into account, this point deserves a more careful and detailed study. Anyhow, Fig. 5 is a clear indication of the difficulties associated with the experimental detection of the meso-shell.

Table 5 Parameters obtained from the simulation analysis entering in the EXAFS equation, Eq. (3) (see text for details)

Shell	N	$\bar{R}$ (Å)	σ^2 (Å^2)
First shell			
Pd^{2+}	4	2.019	0.0017
Pt^{2+}	4	2.021	0.0023
Meso shell			
Pd^{2+}	2	2.780	0.031
Pt^{2+}	2	3.029	0.032
Pd^{2+} [15]	2	2.5	0.015
Second shell			
Cr^{3+} [44]	14	3.97	0.032

For comparative purposes, experimental results from Ref. [15] and Ref. [44] are also included. Envelopes using the parameters here reported are plotted in Fig. 5

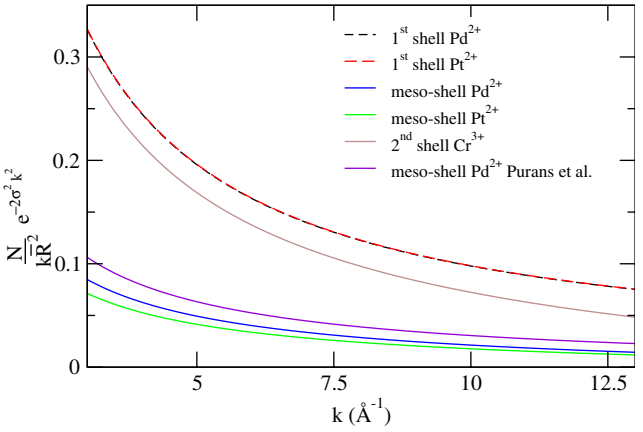

Fig. 5 Different envelopes $\frac{N}{k\bar{R}^2} e^{-2\sigma^2 k^2}$ as a function of the photoelectron wave vector (see text for details)

4 Concluding remarks

Simulation results on the Pt^{2+} hydration reported in this work have shown the presence of two axially located water molecules, as previously found [14] for the Pd^{2+} hydration. In fact, the comparison of palladium and platinum results show how the only major difference between the hydration of both ions, at a structural and dynamic level, is certainly the sharpness of the meso-shell. Palladium ion defines this shell to a larger extent which is more labile in the case of platinum. This difference originates from the interaction energies between the HI and the water molecules occupying this region. In spite of the lability differences, water molecules occupying the meso-shell follows for both ions the same pattern, characterized by frequencies around 150 cm^{-1}. However, the second hydration shell for both cations are noticeably similar. As a consequence, the platinum hydration, compared to that of palladium, amplifies the dynamic differences between the meso-shell and the second hydration shell.

A new feature determined in this work is the translational diffusion coefficient for palladium meso-shell. The value obtained is much closer to that of the ion than to the corresponding of the second hydration shell. This is in sharp contrast with the mean residence times computed for both regions.

The observed differences between palladium and platinum aquaions can give some insights in the mechanistic interpretation of the solvent exchange results at the first hydration shell. The dependence of the exchange rate constant on pressure, what provides the activation volumes $\Delta V^{\neq}$, is one of the most extensively used tools for the experimental determination of solvent exchange mechanisms [17]. Activation volumes found for Pd^{2+} and Pt^{2+} are small and negative (-2.2 and $-4.6\,cm^3$/mol, respectively), which are related to an associative-like mechanism, although the distinction between a limiting associative (**A**) and an associatively activated interchange ($\mathbf{I}_a$) mechanisms is not well established yet [7]. The small activation volumes have been rationalized, but not demonstrated, on the basis of water molecules loosely bound to the metal ion on axial positions [7,8,17–19]. Our microscopic description of the hydration structure and dynamics of Pd^{2+} and Pt^{2+} aqueous solutions support that premise. Previous QM calculations [12] have shown that the pentacoordinated transition state structures for both ions are remarkably close from a structural point of view. If this approach, where outer water molecules are neglected, is valid, the main differences in $\Delta V^{\neq}$ between palladium and platinum should be located at the reactant states. In this sense, the longer distance between the platinum and the meso-shell, compared to palladium, predicts a larger negative value for this ion, in agreement with the observed experimental tendency.

The results presented here lead to the idea that the meso-shell represents a specific pattern of the square planar aquaions hydration. Whether this pattern is still present for other planar species is an open question. To this point, it is worth pointing out that interaction potentials following a strategy similar to that presented here can be applied for other systems, such as $[Au(H_2O)_4]^{3+}$ or $[Cu(NH_3)_4]^{2+}$ or related copper complexes of biochemical interest. Molecular dynamics simulations for those systems in aqueous solutions can then be performed providing accurate information, difficult to extract experimentally, about the (sub)nanosecond dynamics of these systems.

Acknowledgements Junta de Andalucía (FQM282), Spanish DGICYT (BQU2002-02217) and FEDER funds (UNSE-E017) are acknowledged for financial support.

References

1. Marcus Y (1986) Ion solvation. Wiley, Chichester
2. Richens DT (1997) The chemistry of aqua ions. Wiley, Chichester
3. Marcus Y (1997) Ion properties. Marcel Dekker, New York
4. Barthel JMG, Krienke H, Kunz W (1998) Physical chemistry of electrolyte solutions. Steinkopff, Darmstadt
5. Taube H (1954) J Phys Chem 58:523
6. Lippard SJ, Berg JM (1994) Principles of bioinorganic chemistry. University Science Books, California
7. Helm L, Merbach AE (1999) Coord Chem Rev 187:151
8. Erras-Hanauer H, Clark T, van Eldik R (2003) Coord Chem Rev 238–239:233
9. Frank HS, Evans MW (1945) J Chem Phys 13:507
10. Conway BE (1981) Ionic hydration in chemistry and biophysics vol 12. Elsevier, Amsterdam
11. Ohtaki H, Radnai T (1993) Chem Rev 93:1157
12. Deeth RJ, Elding L (1996) Inorg Chem 35:5019
13. Ayala R, Sánchez Marcos E, Díaz-Moreno S, Solé VA, Muñoz-Páez A (2001) J Phys Chem B 105:7588
14. Martínez JM, Torrico F, Pappalardo RR, Sánchez Marcos E (2004) J Phys Chem B 108:15851
15. Purans J, Fourest B, Cannes C, Sladkov V, David F, Venault L, Lecomte M (2005) J Phys Chem B 109:11074
16. Hellquist B, Bengtsson L, Holmberg B, Hedman B, Persson I, Elding LI (1991) Acta Chem Scand 45:449
17. Helm L, Merbach A (2005) Chem Rev 105:1923
18. Richens D (2005) Chem Rev 105:1961
19. Rotzinger F (2005) Chem Rev 105:2003
20. Raber J, Zhu C, Eriksson L (2005) J Phys Chem B 109:11006
21. Zhu C, Raber J, Eriksson L (2005) J Phys Chem B 109:12195
22. Gill DS (1984) Platinum coordination complexes in cancer chemotherapy (Hacker et al., Eds) Martinus Nijhoff Publishing, pp 267–278
23. Pappalardo RR, Sánchez Marcos E (1993) J Phys Chem 97:4500
24. Pappalardo RR, Martínez JM, Sánchez Marcos E (1996) J Phys Chem 100:11748
25. Martínez JM, Pappalardo RR, Sánchez Marcos E (1998) J Chem Phys 109:1445
26. Martínez JM, Pappalardo RR, Sánchez Marcos E (1999) J Am Chem Soc 121:3175
27. Martínez JM, Merkling P, Pappalardo RR, Refson K, Sánchez Marcos E (2004) Theor Chem Acc 111:101
28. Elrod NJ, Saykally RJ (1994) Chem Rev 94:1975
29. Andrae D, Haeussermann U, Dolg M, Stoll H, Preuss H (1990) Theor Chim Acta 77:123
30. Woon D, Dunning THJ (1993) J Chem Phys 98:1358
31. Jorgensen WL, Chandrasekhar J, Madura JD, Impey RW, Klein ML (1983) J Chem Phys 79:926
32. Breneman CM, Wiber KB (1990) J Comp Chem 11:361
33. Miertus S, Scrocco E, Tomasi J (1981) Chem Phys 55:117
34. Mennucci B, Cancès E, Tomasi J (1997) J Phys Chem B 101:10506
35. Refson K (1996) MOLDY User's Manual Rev. 2.10 (Moldy code can be obtained from the CCP5 program library)
36. Refson K (2000) Comput Phys Commun 126:310
37. Allen MP, Tildesley DJ (1987) Computer simulation of liquids. Oxford University Press, Oxford
38. Leslie M, Gillan M (1985) J Phys Condens Matter 18:973
39. Roberts JE, Schnitker J (1995) J Phys Chem 99:1322
40. Figueirido F, Del Buono GS, Levy RM (1995) J Chem Phys 103:6133
41. Bogusz S, Cheatham TE III, Brooks BR (1998) J Chem Phys 108:7070
42. Impey RW, Madden PA, McDonald IR (1983) J Phys Chem 87:5071
43. Stern E (1988) X-Ray Absorbtion: Principles, Applications, Techniques of EXAFS, SEXAFS and XANES (Koningsberger and Prins, Eds.) Wiley-Interscience, New York, p 3
44. Sakane H, Muñoz-Páez A, Díaz-Moreno S, Martínez J, Pappalardo R, Sánchez Marcos E (1998) J Am Chem Soc 120:10397
45. Campbell L, Rehr J, Schenter G, McCarthy M, Dixon D (1999) J Synchrotron Radiat 6:310
46. Merkling P, Muñoz-Páez A, Sánchez Marcos E (2002) J Am Chem Soc 124:10911